Influence of image artifacts on image-based computer simulations of the cardiac electrophysiology

Computers in Biology and Medicine 137 (2021) 104773

Contents lists available at ScienceDirect

Computers in Biology and Medicine

journal homepage: www.elsevier.com/locate/compbiomed

Influence of image artifacts on image-based computer simulations of the cardiac electrophysiology

E. Kruithof [a,*], S. Amirrajab [a], M.J.M. Cluitmans [b,c], K.D. Lau [b], M. Breeuwer [a,d]

[a] Eindhoven University of Technology, the Netherlands
[b] Philips Research Eindhoven, the Netherlands
[c] Maastricht University Medical Center, the Netherlands
[d] Philips Healthcare Best, the Netherlands

ARTICLE INFO

Keywords:
Cardiac phantom
Electrophysiological modeling
Image artifacts
Simulated MR images
Ventricular tachycardia

ABSTRACT

Myocardial infarct patients have an increased risk of scar-based ventricular tachycardia. Late gadolinium enhanced magnetic resonance (MR) imaging provides the geometric extent of myocardial infarct. Computational electrophysiological models based on such images can provide a personalized prediction of the patient's tachycardia risk. In this work, the effect of respiratory slice alignment image artifacts on image-based electrophysiological simulations is investigated in two series of models. For the first series, a clinical MR image is used in which slice translations are applied to artificially induce and correct for slice misalignment. For the second series, computer simulated MR images with and without slice misalignments are created using a mechanistic anatomical phantom of the torso. From those images, personalized models are created in which electrical stimuli are applied in an attempt to induce tachycardia. The response of slice-aligned and slice-misaligned models to different interval stimuli is used to assess tachycardia risk. The presented results indicate that slice misalignments affect image-based simulation outcomes. The extent to which the assessed risk is affected is found to depend upon the geometry of the infarct area. The number of unidirectional block tachycardias varied from 1 to 3 inducible patterns depending on slice misalignment severity and, along with it, the number of tachycardia inducing stimuli locations varied from 2 to 4 from 6 different locations. For tachycardias sustained by conducting channels through the scar core, no new patterns are induced by altering the slice alignment in the corresponding image. However, it affected the assessed risk as tachycardia inducing stimuli locations varied from 1 to 5 from the 6 stimuli locations. In addition, if the conducting channel is not maintained in the image due to slice misalignments, the channel-dependent tachycardia is not inducible anymore in the image-based model.

1. Introduction

In the US, thousands of people suffer from myocardial infarction annually [1]. After their initial infarct, these patients have an increased risk of scar-based ventricular tachycardia (VT) and therefore sudden cardiac death [2]. Myocardial infarction results in areas of non-conducting scar core and damaged tissue with remodeled electrophysiological (EP) properties, referred to as the border zone (BZ). The alterations in EP properties can result in VT, which is sustained by a reentry mechanism where the myocardium re-excites itself by means of an electrical impulse which re-circulates in the myocardium. Such re-entries typically take place in myocardium areas with heterogeneous EP properties such as scar and border zone, and they are therefore highly dependent on infarct scar geometry [3].

As described by Deng et al. [2], reentry mechanisms can be subdivided into two categories as shown in Fig. 1. The first category is the functional block reentry, which is induced by abnormal action potential and refractory periods of the BZ cells, causing a reentry loop along BZ boundaries that results in VT. The second category are conducting channels (CCs) through the non-viable core, which are responsible for 63% of the VTs. These CCs can be classified as I and T type CCs, through which the reentry loop can be sustained. These findings indicate that patient-specific VT risk depends upon individual scar characteristics [3].

According to Ref. [4], myocardial infarct patients have an abundance of CCs, but only a small subset of them result in VT. In Ref. [2] it was reported that the dimensions of the CC are critical for its ability to

* Corresponding author.
E-mail address: e.kruithof@tue.nl (E. Kruithof).

https://doi.org/10.1016/j.compbiomed.2021.104773
Received 11 May 2021; Received in revised form 12 August 2021; Accepted 13 August 2021
Available online 23 August 2021

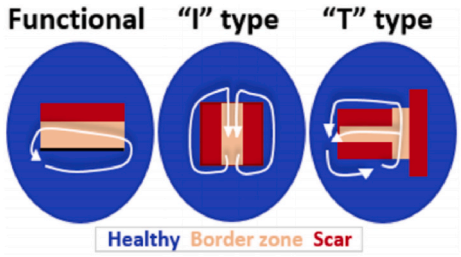

Fig. 1. Three different types of VT as described by Ref. [2]. The white arrows represent the EP wave propagation, which is caught in a loop. The black line represents an EP propagation block.

sustain VT. To understand the functional relationship between infarct geometry and VT emergence, image-based EP models can be created [2]. [5] in which the patient-specific scar geometry can be obtained from contrast enhanced magnetic resonance (MR) images. For such image-based models, accurate reconstruction of the patient's infarct geometry is key for the prediction of the VT risks. It is demonstrated that 70% of the CCs detected in invasive electroanatomic maps can be reconstructed from high-resolution contrast enhanced MR images [4], but the image quality may affect the reconstructed results. For example, in Ref. [6] it was demonstrated that differences in image resolution shift the simulated reentry path by 11 mm on average. However, to our knowledge, the effect of respiration image artifacts on such EP models remain uncharacterized.

In the clinic, LGE images are typically created as a stack of multiple 2D (M2D) short axis (SA) slices, which results in M2D SA LGE MR images with a coarse out-of-plane spacing of 5–12 mm [7]. According to Ref. [8], misalignment artifacts of M2D MR slices are inevitable and reported to be as large as 18 mm, with an average of 5 mm. These artifacts are the result of respiratory motion of the heart, which can cause translations and rotations in the MRI slices.

In this study, the effect of slice misalignment on reconstruction of scar geometry and the resulting EP simulation outcome will be further investigated. To this end, both aligned- and misaligned-image-based EP simulations are required. However, the aligned ground truth for the clinical slice misaligned LGE images is unknown and it can be challenging to account for respiratory motion artifacts [9]. Therefore, we have utilized the mechanistic 4D eXtended CArdiac Torso (XCAT) phantom [10] to generate simulated LGE MR images with and without respiratory slice alignment artifacts, which represent a LGE MR image with common alignment artifacts and the ground truth respectively. Personalized 3D computer models of the cardiac EP are created from both a clinical and a XCAT simulated LGE MR dataset, which contain scar with and without I type CC respectively.

This paper starts with a motivation for and a description of the performed experiments. The image-to-EP-model pipeline (Fig. 2) is discussed in further detail as well. Finally, the responses of both slice aligned and slice misaligned image-based models from various applied electrical stimuli are explored.

2. Methods

In this work, the influence of misalignment between the M2D LGE MR SA slices on scar reconstruction and the resulting EP simulation is explored. Our hypothesis is that the influence of such alignment artifacts depends on misalignment severity and on the VT type as well: we expect that functional block VT models will be more robust for slice alignment artifacts than VTs sustained by conducting channels, as such channels are small structures and therefore more easily disturbed by slice misalignment. Functional block VT can occur in larger BZ tissue volumes and is caused by the difference between BZ and healthy tissue EP properties. The geometry of such functional block inducing infarcts varies significantly, therefore it is expected that small geometric differences caused by slice misalignment will not necessarily prevent the VT of being induced. However, for the VTs that rely on CCs, a more significant impact of slice misalignment on EP simulation outcome is expected. According to Ref. [2], CCs with a channel length of 2 cm and a diameter of 0.5 cm are most critical; such CCs are often able to sustain induced VTs as illustrated in Fig. 1. Since a VT sustaining CC is only a small structure, we expected that a small slice misalignment could alter the reconstructed geometry and therefore the simulated outcome. If the misalignment is too large, the reconstructed channel geometry could be blocked with core tissue inhibiting VT. In addition, slice misalignment artifacts can affect channel length and this could also significantly affect the EP simulation as channel length also determines whether VT can be sustained or not 2. For these reasons, both types of VT are studied by examining the influence of slice misalignment on EP simulations based on LGE images containing scar with and without a CC.

For functional block VT simulations, clinical LGE MRI data containing scar without a CC was available (Sec. 2.1). This MR image contains slice misalignment artifacts and slice thickness (SLT) that are common in the clinic. For I type VT simulations, multiple LGE images containing CC scar are simulated from the XCAT phantom (Fig. 4). The first advantage of using the XCAT phantom is that the SLT and respiratory slice misalignment artifacts can easily be controlled, such that both LGE images with and without artifacts are created. Moreover, a high-resolution image without respiratory artifacts is simulated as

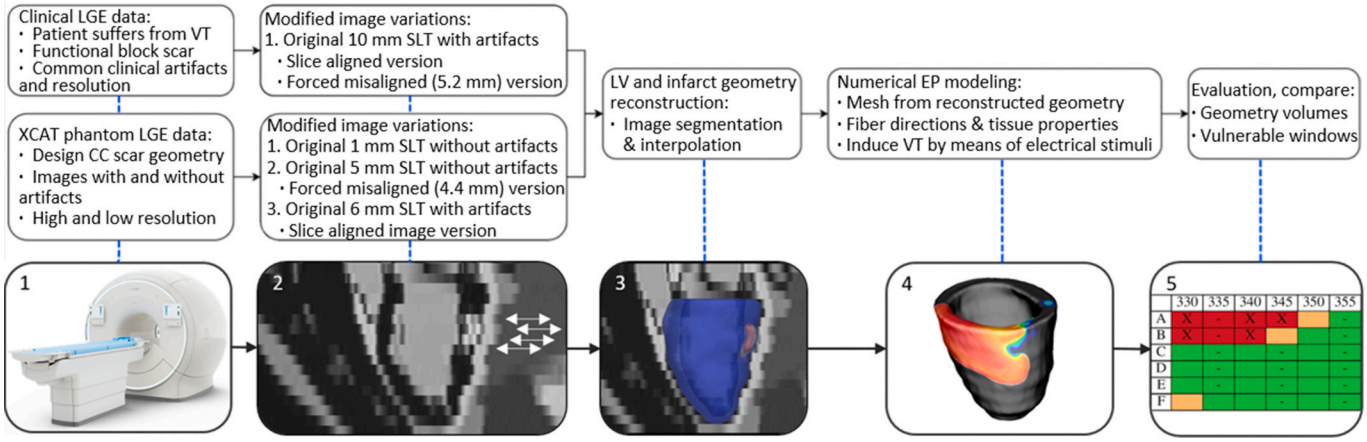

Fig. 2. Five successive steps, starting from a MR LGE image, to assess VT s by EP modeling. Step 1: Create LGE MR images. Step 2: Use slice translations to correct for or induce slice misalignments. Step 3: Reconstruct LV and infarct geometry from the (modified) LGE image. Step 4: Create numerical EP model and attempt to induce VT. Step 5: Use simulation results to examine VT risk and slice misalignment effects.

ground truth, a factor that is missing from the clinical dataset. The second advantage of using the XCAT phantom is that a scar geometry can be designed with most critical dimensions and added to its LV. In this way, we know that the EP simulation based on the image without respiratory artifacts should have a high risk of developing VT. In addition, it can be investigated whether slice misalignment alters the indicated risk, which is undesired as an incorrect risk indication can lead to the wrong treatment decision for this virtual patient.

To investigate the influence of slice misalignment on reconstructed geometries and EP simulation outcome, several experiments are performed. EP models are created from LGE images with respiratory artifacts, and from their modified versions in which in-plane misalignments are corrected for. Additionally, a forced misaligned version of the image is created in which the misalignment of one of the slices is adjusted to reproduce the reported average LGE slice misalignment of 5 mm such that the influence of the most common misalignment magnitude on EP simulation outcome can be investigated as well. Simulated EP outcomes based upon the different images, including the ground truth image, are compared to each other to investigate the influence of the image artifacts. Table 1 summarizes all experiments.

Once all LGE images and their modified versions are created, the image-based EP simulations are performed. Two series of image-based EP models are created, the first series is based on the clinical image and its modified versions; the second series is based upon the XCAT simulated LGE images and their modified versions. The EP models are created following five steps as illustrated in Fig. 2, which are discussed in more detail in the following sections.

Table 1
Overview of the five MR images, their modified versions and how those are used in the experiments.

Scanner protocol Image description	Pixel spacing [mm]	Modified image version	Purpose
Clinical cine MRI	[0.911 0.911 10.00]	Unmodified	Semi-automatic LV contouring in the LGE by image to image registration.
Clinical LGE M2D SA Low-resolution & misalignments	[0.879 0.879 10.00]	Unmodified	Explore influence of slice misalignments (3.5 mm) on functional block EP results.
		Modified – all slices aligned	Explore influence of slice alignment on functional block EP results.
		Modified – 1 slice forced misaligned	Explore influence of reported average misalignment (5 mm) on functional block EP results.
XCAT LGE M2D SA High-resolution	[0.738 0.738 1.00]	Unmodified	Used to create ground truth I-type EP results.
XCAT LGE M2D SA Low-resolution	[0.738 0.738 5.00]	Unmodified	Explore I-type EP results for an image without alignment artifacts.
		Modified – 1 slice forced misaligned	Explore influence of reported average misalignment (5 mm) on I-type EP results.
XCAT LGE M2D SA Low-resolution & misalignments	[0.880 0.880 6.00]	Unmodified	Explore influence of slice misalignments (3.5 mm) on I-type EP results.
		Modified – all slices aligned	Explore influence of slice alignment on I-type EP results.

2.1. Clinical and simulated MR dataset

2.1.1. Clinical dataset

Clinical MR images of a 40 year old male patient are used who developed frequent premature ventricular complexes of three different types during an isoprenaline provocation test. In this study, a M2D SA LGE MR image is included, which was acquired on a Philips 1.5T Ingenia scanner (Gradient Recalled MAG Prepared sequence, TR: 6.11 ms, TE: 2.998 ms, FA: 25°, 0.879 × 0.879 mm voxel resolution, 8 mm SLT, 10 mm slice spacing). This image contains common clinical respiratory artifacts and SLT (Fig. 3). In addition, the multi-slice multi-phase SA functional cine MR image (TR: 3.26 ms, TE: 1.63 ms, FA: 60°, 0.911 × 0.911 mm voxel resolution, 8 mm SLT, 10 mm slice spacing, 210 phase encoding steps) of the heart was imported into Philips IntelliSpace Portal [11] for semi-automatic LV segmentation in the LGE image by means of image registration. The patient provided written informed consent and the study has been approved by the Medical Ethical Committee of the Maastricht Academic Hospital (Maastricht, The Netherlands).

2.1.2. Simulated dataset

The simulated data is created by utilizing the mechanistic 4D XCAT non-infarcted heart model as an anatomical phantom [10]. This model is extended with a cylindrically shaped scar with outer and inner layers for the BZ and I type CC. The scar is approximately placed at the same location as the infarct in the clinical dataset; it is located around the right coronary artery in the left ventricle (LV) wall, 2 cm below the SA valve plane (Fig. 5). The scar has an elliptical cross section and a length of 20 mm. The minor and major diameters are 10 and 20 mm for the BZ, 8 and 16 mm for the scar core and 3 and 6 mm for the CC (Fig. 5). The dimensions of the scar and CC are chosen such that they match the average characteristics for critical CCs as described in Ref. [2], which are defined as VT sustaining CCs.

Bloch-equation based MR image simulation is performed to generate M2D SA LGE images as introduced by Ref. [12] (TR: 3 ms, TE: 1.5 ms, FA: 40°, TI: 678 ms). Two images are created without respiratory artifacts with SLT of 1 and 5 mm (0.738 × 0.738 mm voxel resolution) of which the former is used as ground truth (Fig. 4B&C). A third 6 mm SLT image containing respiratory artifacts is created as well (0.88 × 0.88 mm voxel resolution). Slice misalignments in clinical images are caused by movements of the heart due to breathing. This effect is mimicked in the XCAT image by acquiring the slices at the same point in the cardiac cycle, but at slightly different time points in the breathing cycle in the XCAT motion model. The total duration of the breathing cycle is set to 5 s and the movement of the heart during breathing is set to 0.5 cm in-plane and 1.0 cm out-of-plane resulting in misalignment artifacts up to 3.5 mm which is similar to those in the clinical LGE image (Fig. 4D).

2.2. Image modifications

The image modifications are based upon the LV wall contours created with the Philips IntelliSpace Portal workstation. For each LV containing slice, the LV centroid point of that slice is detected. Through

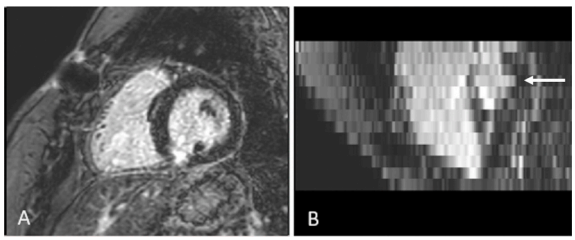

Fig. 3. A) Clinical LGE data with enhanced infarct tissue around right coronary artery (SA view). B) The multiple SA slices contain respiratory misalignments (white arrow) and cause a low out-of-plane resolution (LA view).

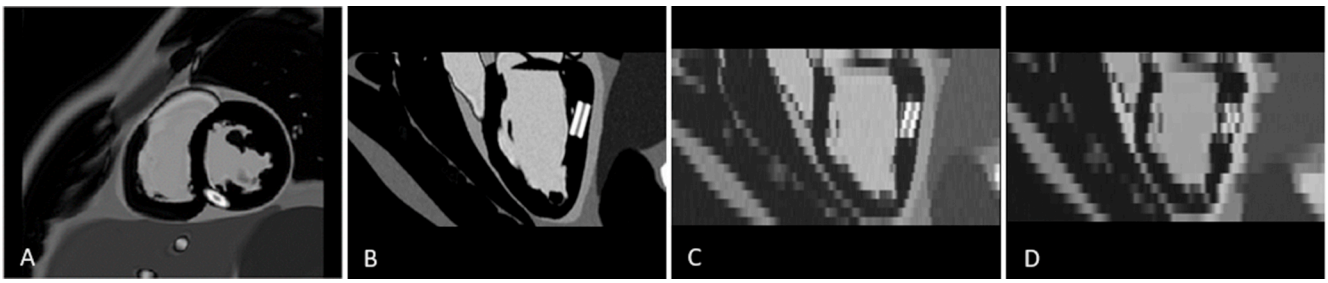

Fig. 4. A) SA view of simulated M2D SA LGE MR image with enhanced scar located around right coronary artery. LA view of B) 1 mm SLT and C) 5 mm SLT simulated LGE image without respiratory and D) 6 mm SLT image with respiratory artifacts.

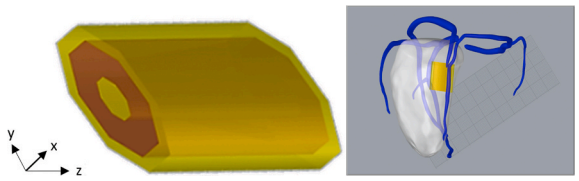

Fig. 5. Designed CC scar geometry for XCAT heart phantom. The scar core is visualized in red and the BZ and CC in yellow.

those points, a smooth cubic B-spline is fitted to represent the aligned centroid of the LV in 3D space. The slice aligned image version is created by translating each slice by the in-plane displacement required to align the LV centroids of each slices with the smooth spline. Secondly, forced misaligned image versions are created for which one slice is chosen, here the slice closest to the VT origin, which is translated in-plane to create a misalignment which approximates the reported average of 5 mm. For the simulated data, the direction of the 4.4 mm translation is chosen by trial and error such that the structure of the CC maintained a continuous channel. For the clinical data, the chosen slice is translated such that the original misalignment of 3.5 mm is increased to 5.2 mm, where the misalignment magnitude is obtained by comparing the image to the slice-aligned image version. An overview of the original and modified images is given in Table 1.

2.3. Geometrical model construction

Once the desired slice alignment is obtained, the LV and infarct in the resulting image are segmented. The cine image is used to automatically segment endocardial and epicardial contours in IntelliSpace Portal. In IntelliSpace, these contours are registered to the LGE image where they are used to create a myocardial mask by selecting pixels that belong to the myocardium. The resulting myocardium mask is used to restrict the image analysis methods to the myocardium area only. The infarct area is segmented following a standard deviation-based thresholding approach [13]. Pixels with intensities above the median intensity +1.5 standard deviation within the myocardium image histogram are classified as infarct tissue. Within the total infarct tissue, the infarct core is defined as the pixels with intensities above median intensity +1 standard deviation within the infarct region. Segmentations of single pixels are removed as they are considered as noise.

To reconstruct the infarct geometry, parts of the approach described by Ref. [7] are utilized. Following this method, the infarct binary label map is smoothed using image convolution with the Gaussian kernel with $\sigma = 3$. As a result, each pixel is assigned a value in the interval [0, 1], which is interpreted as its probability to belong to the infarct region. A third-order spline interpolation is then used to create an interpolated 3D probability map. This map is thresholded using a threshold value of 0.5 to generate an interpolated 3D reconstruction of the total infarct region. The same approach is applied to the infarct core label map and finally, the border zone geometry is created by subtracting the core from the total infarct geometry. As last, the LV geometry is reconstructed from the contours of the LGE SA slices, which are interpolated in order to create the LV surface. The result is manually extended to add the apex using the 3DSlicer segment editor [14]. The resulting volumetric geometries are used to create and label the numerical mesh, as described in the following section.

2.4. Computational modeling

2.4.1. Electrophysiological modeling

Using the image-based volumetric geometries, finite-element tetrahedral meshes are generated with an average resolution of 480 μm. Monodomain EP simulations are performed in the CARP modelling framework (https://carpentry.medunigraz.at/carputils) using the Crank-Nicolson time integrator (20 μs time step) and the Ten Tusscher ionic model for human ventricular myocytes [15]. In this work, the ionic model is adapted to account for the remodeled cell properties of the BZ and CC. The ion channel conductances of the BZ and CC regions are reduced by the following percentages: sodium current (GNa) −62%, L-type calcium current (GCaL) −69%, potassium currents (Gkr) −70%, (GK1) −50% and (Gks) −80%. This causes an elongation in action potential duration, decreased upstroke velocity and decreased peak amplitude compared with the non-infarcted myocardium (Fig. 6). The myocardial fiber architecture is assigned using a rule-based method as described in Ref. [16]. The anisotropic conduction values are then tuned using the methods of [17] to match a conduction velocity of 0.6 m/s along the myocardial fibers and 0.3 m/s transverse to them. For the BZ and CC, transverse conductivity is reduced by 90% to reflect tissue remodeling in these pathological regions [3]. The conductivity values for the non-viable core were set to approximately zero.

2.4.2. Pacing protocol

LV EP simulations are performed by pacing six different locations on the endocardium equally distributed around the infarct at a distance of approximately 2 cm [18]. At those locations (Fig. 7), baseline pacing of 6

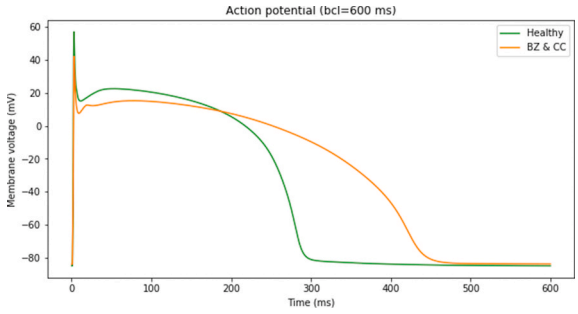

Fig. 6. Transmembrane voltage over time within the single cell for the Ten Tusscher ionic model. Ionic modifications for the infarct areas causes an elongation in action potential duration (418 ms vs 324 ms), decreased upstroke velocity and peak amplitude compared with the healthy myocardium.

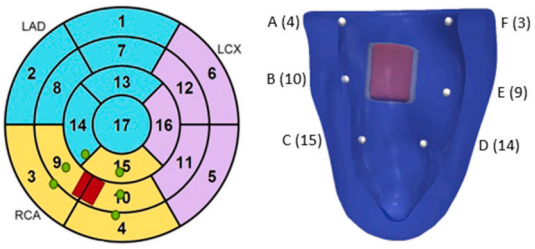

Fig. 7. Visualization of the infarct (red) and pacing locations (A–F) in AHA segment model and in the reconstructed geometry with reference; to the AHA segment numbers.

stimuli (S1) with cycle length of 600 ms is performed, followed by a premature stimulus (S2) in order to induce VT [2]. A range in S1–S2 time intervals (330–370 ms) is used in an attempt to induce VT. Each stimulus has a duration of 2 ms, an amplitude of 40 μA/cm^2 and a diameter of 3 mm.

2.5. Evaluation methods

For each model, the myocardial and infarct volumes are calculated from the volumetric geometry surfaces. Additionally, simulation outcomes are captured in vulnerable windows (VW) that defines for each model and pacing location the S1–S2 time intervals at which VTs are induced. Here a VT is defined when electrical activity was sustained for 1200 ms or longer after S2. S1–S2 time intervals are adjusted by 10 ms for each new simulation. In case one of two consecutive 10 ms interval simulations result in sustained VT, an additional simulation is performed with a 5 ms S1–S2 interval adjustment to more exactly determine the time interval range for which VT can be induced. Other simulations with 5 ms interval difference are assumed to give similar results as its closest 10 ms interval simulations. Those assumed results are indicated with an '-'. Finally, reentry exit points are defined and detected as the point with earliest second activation time, counted from the start of the S2 stimulus. The results are evaluated by comparing VWs, geometrical volumes and reentry exit points for unmodified, slice aligned, forced misaligned and ground truth models with each other.

3. Results

3.1. Clinical model series

The clinical model series contains three model variants based on the same LGE image. One model was created from the original image in which maximal misalignment of 3.5 mm was found in slice 6, which is indicated with a black dashed box in Fig. 9. This misalignment was further increased to 5.2 mm in the forced misaligned model and in the aligned reconstruction, the in-plane misalignments are corrected for (Fig. 9). The LV and infarct volumes are on average 101.2 cm^3 and 6.5 cm^3 respectively. The infarct is further divided into 5.0 cm^3 BZ and 1.5 cm^3 core. For the three models, the absolute differences in volumes is small, but improving the alignment of the image resulted in an increased infarct volume up to 1 cm^3.

During the EP simulations, three different functional block reentry patterns are observed and labeled as reentry *X*, *Y* and *Z* (Fig. 10). In Fig. 8 the transmembrane voltage is used to visualize reentry type *X*, which was inducible in all model variants. The other two reentry types were less common as seen in Table 2. The distance between exit points of the three reentry types is 28 mm (X–Y), 30 mm (X-Z) and 49 mm (Y-Z). Shifts in exit point locations are observed when a different stimulation location or geometry reconstruction was used. The amplitude of those shifts was in both cases in range of 1–10 mm.

VWs are determined for a S1–S2 interval range of 330–370 ms in which the induced reentry patterns are indicated as well (Table 2). The X-reentry is the most prevalent one; in the slice aligned model, it was the only pattern that could be induced for 2 out of 6 pacing locations. However, in the unmodified model the less prevalent Y-reentry appears as well. In the forced misaligned model, a third reentry pattern (Z) is induced as well, which blocked and took the place of the X-reentry induced at pacing location A for S1–S2 interval of 330 and 340 ms. In addition to the type of inducible reentry patterns, also a difference in the amount of pacing locations for which reentry is induced was found. In the realigned model, VT was found for location A and B only. However, in the unmodified model location F resulted in VT as well and in the forced misaligned model, even a fourth pacing location, C, resulted in VT.

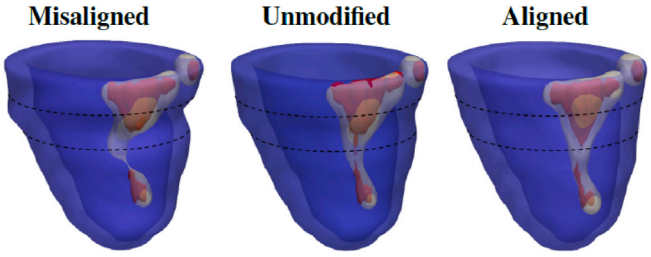

Fig. 9. Reconstructed geometries for the three clinical model variants.

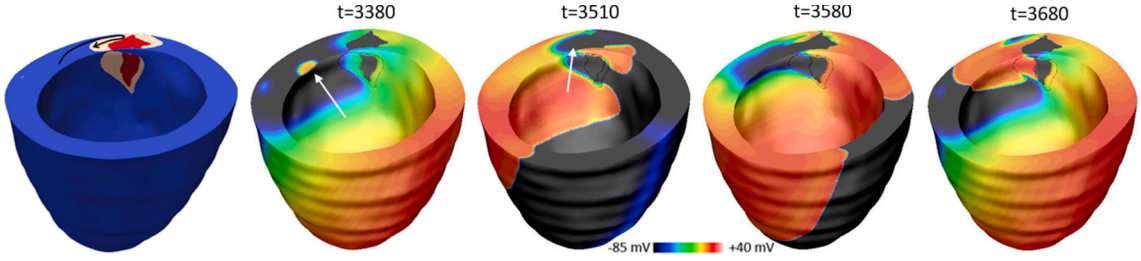

Fig. 8. Clipped model visualization of the EP wave propagation from pacing location A (white arrow at t = 3380 ms) towards the depolarized BZ area causing a functional block (white arrow at t = 3510 ms). However, approximately 70 ms later the BZ is repolarized, allowing the EP wave to propagate backwards through the BZ area. Overview of the pattern is given with the black arrow in the leftmost image. In this label map, the blue color indicates healthy myocardium. Yellow the BZ and red the infarct core.

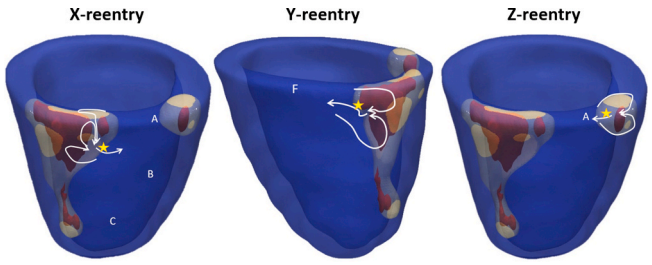

Fig. 10. Overview of three functional block reentries induced in the clinical models as illustrated with the white arrows. Yellow stars illustrate their corresponding exit points. Reentry X is induced for pacing location A-C. reentry Y for pacing location F and reentry Z for pacing location A.

3.2. XCAT model series

The XCAT model series contains five model variants of the same virtual patient based on three different simulated LGE images. This series covers models based on a slice aligned, unmodified and forced misaligned LGE image variants and in addition, unlike the clinical series, two models based on unmodified images without respiratory artifacts are included as well. Slice alignment artifacts affected the width, length and shape of the CC as shown in Fig. 11. The calculated LV and infarct volumes are on average 102.1 cm^3 and 2.3 cm^3 respectively. An increased slice alignment resulted in an increased reconstructed infarct volume. In addition, higher image resolution yields the same effect. However, absolute volume differences are again small with a maximum difference of 0.3 cm^3.

The XCAT VWs can be categorized into three states as illustrated in Table 3. Whether VT is inducible or not depends on the S1–S2 interval, because this determines the available time for the CC tissue to repolarize. If this interval is too short (state 1), the EP wave is blocked at both entrances and if this interval is too long (state 3), the EP wave enters the CC from both sides canceling each other in the middle of the CC. Between these extremes, a range of S1–S2 intervals can be found for which the EP wave is blocked at only one of the CC entrances, resulting in I type VT (state 2) as illustrated in Fig. 12. In the simulation outcomes, two different I type VT patterns are observed. The *U* pattern is defined as I type VT for which the re-entering EP wave propagates upwards through the I channel in contrast to the *D* pattern, where it propagates downwards through the CC (Fig. 13). Reentry exit points overlap with the CC entrances.

From the VWs corresponding to the images without respiratory artifacts can be seen that 5 out of 6 pacing locations resulted in VT, which indicates a high VT risk for this patient. It should be noted that pacing location B in the 1 mm SLT model generated both state 1 (S2 = 330–365 ms) and state 3 (S2 = 370 ms) simulation outcomes. It is expected that state 2 results (VT) can be created with an S1–S2 interval between 365 and 370 ms. The small width of state 2 in this window is caused by the fact that both CC entrances have the same width in the high-resolution model (Fig. 11), and the distances from the CC entrances to pacing

Table 2
VWs indicating for each clinical model, pacing location and S1–S2 interval if VT is induced or not. VTs sustaining for at least 1200 ms are indicated in red, others in yellow. For the green blocks, no reentry was induced. In addition, the reentry type (XYZ) is indicated in each red block. '-' results are interpolated from other simulations.

10 mm SLT one slice forced misaligned (5.2 mm)

	330	335	340	345	350	355	360	365	370
A	Z	-	Z			-		-	
B	X	-	X	X		-		-	
C	X	-	X			-		-	
D		-		-		-		-	
E		-		-		-		-	
F		Y		-		-		-	

10 mm SLT unmodified with respiratory artifacts

	330	335	340	345	350	355	360	365	370
A	X	-	X			-		-	
B	X	-	X	X		-		-	
C		-		-		-		-	
D		-		-		-		-	
E		-		-		-		-	
F	Y			-		-		-	

10 mm SLT all slices aligned

	330	335	340	345	350	355	360	365	370
A	X	-	X	X		-		-	
B	X	-	X			-		-	
C		-		-		-		-	
D		-		-		-		-	
E		-		-		-		-	
F				-		-		-	

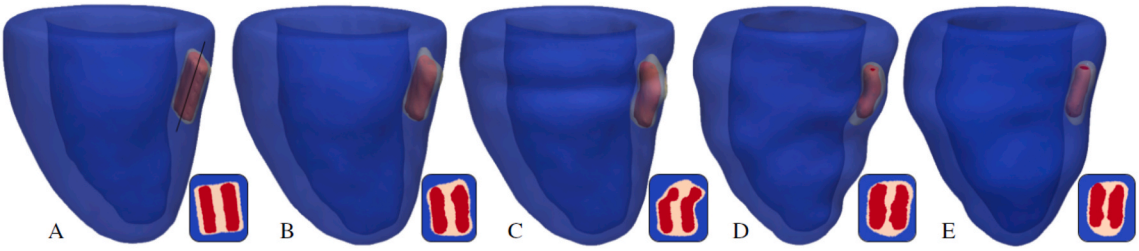

Fig. 11. 3D visualization of the A) 1 mm SLT model without respiratory artifacts, B) 5 mm SLT model without respiratory artifacts, C) 5 mm SLT forced misaligned model, D) 6 mm SLT model with respiratory artifacts, E) 6 mm SLT aligned model. For each model a cross-sectional view through the CC is given using a clipped plane (black line first model) through their CC.

Table 3
VWs indicating for each XCAT model, pacing location and S1–S2 interval if a 1200 ms sustaining VT is induced (red) or not (green). In addition, for the red blocks is indicated if I-type reentry U or D was induced. The VWs can be categorized in three phases. State 1: EP wave is blocked at both CC entrances due to a short S1–S2 interval. State 2: EP wave is blocked at one CC entrance resulting in VT. State 3: EP wave is able to enter CC at both entrances due to a long S1–S2 interval. They cancel each other out in the middle of the CC such that no VT is induced. '-' results are interpolated from other simulations.

1 mm SLT unmodified without artifacts (gt)

	330	335	340	345	350	355	360	365	370
A		-		-			U	-	U
B		-		-		-			
C		-		-		-		D	D
D		-		-		-		D	D
E		-		-		-			U
F		-		U	U	-	U	-	U

5 mm SLT unmodified without artifacts

	330	335	340	345	350	355	360	365	370
A	U	-	U	-	U	-	U		
B	U	-	U	-	U			-	
C	D	-	D	-	D	D		-	
D	D	-	D	-	D	-	D		
E		-		-		-		-	
F	U	-	U	U		U	U	U	

5 mm SLT one slice forced misaligned (4.4 mm)

	330	335	340	345	350	355	360	365	370
A		-		-		-		-	
B		-		-		-		-	
C		D	D			-		-	
D		-		-		-		-	
E		-		-		-		-	
F		-		-		-		-	

6 mm SLT unmodified with respiratory artifacts

	330	335	340	345	350	355	360	365	370
A			U	-	U	-	U		
B		-		U	U			-	
C		-		-		-		-	
D		-		-			D	D	
E	U	-	U	U		-		-	
F	U	-	U	-	U			-	

6 mm SLT all slices aligned

	330	335	340	345	350	355	360	365	370
A	U	-	U	U		-		-	
B		-		-		-		-	
C		-		-		-		-	
D		-		-		-		-	
E	U	-	U	-	U	U		-	
F	U	-	U	-	U	-	U		

	State 1			State 2				State 3	
VW									

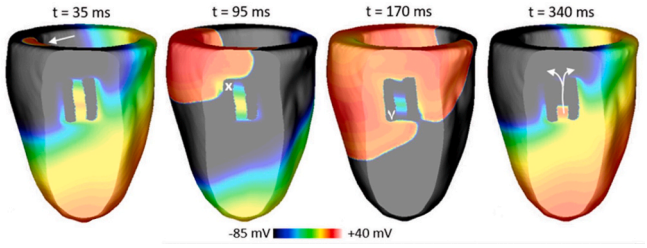

Fig. 12. Transmembrance voltage maps showing I type VT in XCAT model. S2 stimulus at location F (arrow at t = 35 ms) cause EP block at CC entrance closest to the pacing location (x at t = 95 ms). The EP wave enters second CC entrance (v at t = 170 ms) causing I type reentry (aroows at t = 340 ms).

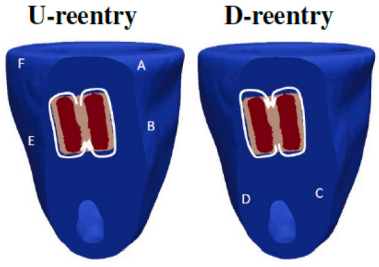

Fig. 13. Two different I-type reentries are induced in the XCAT model. Reentry U is inducible for pacing location A, B, E and F. Reentry D is inducible for pacing location C and D. The white arrows represent the EP propagation pattern causing the VTs.

location B are equal as well. Therefore, both CC entrances need the same amount of time to repolarize and they receive the same amount of time before the next impulse arrives. Thus they will respond in the same way to the S2 stimulus and this makes it more likely to create state 1 and 3 results. In all other models, non-VT inducing pacing locations created state 3 results throughout the whole window. For the VT inducing pacing locations, the relationship between the pacing location used and induced reentry pattern, U or D, is the same in all models. However, slice misalignments resulted in fewer pacing locations to result in VT.

4. Discussion

4.1. Clinical model series

The clinical results demonstrate a significant difference in EP simulation outcomes based upon the MR image and its modified versions. Firstly, the number of functional block reentry patterns inducible from the chosen stimuli locations was determined by the slice alignment. Increasing the slice alignment decreased the number of inducible reentry patterns. In the slice-aligned model, only the X-reentry pattern was induced, which was most prevalent in all clinical models, while in the unmodified model Y-reentry was inducible as well (Table 2). Slice misalignment induced a third reentry type (Z) which was not observed in the other models. It should be noted that the geometry of the infarct region where Z-reentry originated was not affected by the slice alignment modifications; it was the healthy myocardium geometry below this region that changed. This affected the path of EP wave propagation and created the possibility to induce Z-reentry, even though the scar geometry was still the same. In addition, from the VWs it can be concluded that the induced Z-reentries prevented the X-reentry from being induced. These findings show that both smaller (3.5 mm, unmodified) and average (5.2 mm, forced misaligned) in-plane slice misalignments can cause inconsistencies in the amount of inducible reentry patterns. Moreover, the more severe misalignments affected the VW more significantly in terms of inducible reentry patterns compared to the slice-aligned simulation. Therefore, misalignments may affect ablation treatment decisions because the distance between the reentry exit points (28–49 mm) was bigger than typical ablation lesion size [2].

Secondly, a difference in the amount of pacing locations for which VT could be induced was found. The larger the misalignment between the LGE slices, the more pacing locations resulted in VT. This finding shows that both average and smaller slice misalignments in LGE MR images can affect the VT risk assessed through image-based EP

modeling. However, spatial variation in the exit point locations caused by using a different pacing location were in the same range as variations caused by different slice alignment, indicating that these image artifacts do not affect the robustness of reentry location detection by image-based modeling methods.

4.2. XCAT model series

The indicated VT risks for the XCAT ground truth model are high, which was expected since a CC with most critical dimensions was included. The results of the non-ground truth models all differed from the ground truth results, which indicates that image quality does influence the image-based simulation outcome, also previously shown by Ref. [6]. Although the variation in volume was small, the resulting effect upon the EP simulations was substantial. Firstly, a shift in VT inducing stimuli towards shorter S1–S2 intervals can be seen for increased SLT (Table 3). This shift is caused by partial volume effects in these low-resolution images, which enlarges the reconstructed CC width compared to the high-resolution image result. This reduces the delay in CC tissue repolarization and the low-resolution image-based model is therefore more vulnerable to a S2 stimulus at a shorter time interval.

Secondly, a significant difference in results is observed when comparing the forced misaligned model to the unmodified model, which are both based upon the 5 mm SLT image without respiratory artifacts. The forced misalignment reduced the amount of VT inducing pacing locations from 5 to 1 out of 6. The U-reentries for location A, B and F in the unmodified model are caused by EP wave block at the upper side of the CC. The CC shape at this side is affected by the forced misalignment (Fig. 11) such that EP block did not occur anymore, eliminating all U-reentries for this model. From this experiment, it can be concluded that the reported average LGE slice misalignment can drastically affect the predicted risk for VT sustained by CCs. This is especially the case when slice misalignment causes an occlusion in the reconstructed CC such that electrical activity cannot pass through the CC, which is needed to induce the I type VT.

Finally, from the unmodified models based upon low-resolution images with and without respiratory artifacts, it can be observed that respiratory artifacts decreased the CC length from 2.0 to 1.7 cm due to out-of-plane movements of the heart. Because of this, the length deviates slightly from the critical CC dimensions as reported in Ref. [2] (Figs. 11 and 4B&C vs D). For both models, 5 out of 6 pacing locations resulted in VT. However, the respiratory artifacts caused the D-reentry to be less prevalent and the S1–S2 interval ranges inducing VT are smaller. This indicates a less critical CC then in the model without respiratory artifacts, which was expected due to shortening of the CC.

From both model series it can be observed that VWs are significantly affected by slice misalignments as discussed above. Although the effect of slice misalignment on simulations of T-type VTs (see Fig. 1) is not investigated in this study, we expect similar effects as observed with I-type VTs, as both types are sustained by small conducting channels. However, if the misalignment only affects one of the two channel arms, model-assessed VT risk will remain more similar to the ground truth simulation as it can be sustained by the unaffected channel. From the results can be concluded that the application of slice alignment methods for image-based EP models can increase the robustness of the simulation outcome. Here both the misalignment severity and the VT type must be considered when assessing VT form image-based EP models as results show that more severe misalignments cause bigger discrepancies in the VW compared to the aligned simulation results (Table 2) and VWs of functional block and I-type VTs are affected in different ways.

In this study it was observed that the effect of slice misalignment affected simulation outcomes more significantly than variations in SLT. Although differences in SLT can cause small differences in exit points, the reentry patterns remain similar according to Ref. [6]. However, for slice mis-aligned simulations, new reentry patterns were observed which could not be induced in the model with aligned slices, even though multiple pacing locations were used. Therefore, correct slice alignment is a critical factor for model-based VT risk assessment. In this study only in-plane alignments have been tested (Section 2.2) and as illustrated in Table 3, such corrections were not sufficient to correct for VW differences caused by respiratory image artifacts. In future research, the effects of more advanced slice aligning methods including out-of-plane alignments should be studied.

5. Conclusion

We conclude that both average (5 mm forced misaligned) and smaller slice misalignments (3.5 mm) affect EP simulation results in both LV model series, one containing scar with a CC (i.e. I type VT) and one containing scar without a CC (i.e. functional block VT). In the model without a CC, slice misalignment alters the amount of inducible reentry patterns and the amount of VT inducing pacing locations for functional block VTs. For the model with a scar containing a CC, slice misalignment did not result in new reentry patterns but it changed the assessed VT risk by altering the reconstructed CC length and width, geometric factors critical for the assessment of VT risk. Those factors can easily be affected by slice misalignment, and therefore especially the results of models containing a CC are vulnerable for slice misalignment artifacts. It can be concluded that in image-based EP models, misalignments need to be corrected for to increase the robustness of model-based VT risk assessment. Furthermore, more advanced slice alignment methods are recommended as in-plane translations only do not sufficiently correct for respiratory slice misalignment artifacts.

Declaration of competing interest

None declared.

Acknowledgements

This research is a part of the openGTN project, supported by the European Union in the Marie Curie Innovative Training Networks (ITN) fellowship program under project No. 764465 (website: opengtn.eu). M. J.M. Cluitmans is supported by a Veni grant from the Netherlands Organization for Scientific Research (TTW16772). The study sponsors had no involvement in the project design.

References

[1] H.D. White, D.P. Chew, Acute myocardial infarction, Lancet 372 (9638) (2008) 570–584.
[2] D. Deng, A. Prakosa, J. Shade, P. Nikolov, N.A. Trayanova, Characterizing conduction channels in postinfarction patients using a personalized virtual heart, Biophys. J. 117 (12) (2019) 2287–2294.
[3] H.J. Arevalo, F. Vadakkumpadan, E. Guallar, A. Jebb, P. Malamas, K.C. Wu, N. A. Trayanova, Arrhythmia risk stratification of patients after myocardial infarction using personalized heart models, Nat. Commun. 7 (1) (2016) 1–8.
[4] J. Fernández-Armenta, A. Berruezo, D. Andreu, O. Camara, E. Silva, L. Serra, V. Barbarito, L. Carotenutto, R. Evertz, J.T. Ortiz-Pérez, et al., Three-dimensional architecture of scar and conducting channels based on high resolution ce-cmr: insights for ventricular tachycardia ablation, Circulation 6 (3) (2013) 528–537.
[5] K.D. Lau, A. Groth, I. Waechter-Stehle, U.C. Nguyen, P.G. Volders, J. Heijman, J. Weese, M.J.M. Cluitmans, "Personalized Ventricular Arrhythmia Simulation Framework to Study Vulnerable Trigger Locations on Top of Scar Substrate," in 2019 Computing in Cardiology (CinC), IEEE, 2019, p. 1.
[6] D. Deng, H. Arevalo, F. Pashakhanloo, A. Prakosa, H. Ashikaga, E. McVeigh, H. Halperin, N. Trayanova, Accuracy of prediction of infarct-related arrhythmic circuits from image-based models reconstructed from low and high resolution mri, Front. Physiol. 6 (2015) 282.
[7] E. Ukwatta, H. Arevalo, M. Rajchl, J. White, F. Pashakhanloo, A. Prakosa, D. A. Herzka, E. McVeigh, A.C. Lardo, N.A. Trayanova, et al., Image-based reconstruction of three-dimensional myocardial infarct geometry for patient-specific modeling of cardiac electrophysiology, Med. Phys. 42 (8) (2015) 4579–4590.
[8] S. Dangi, C.A. Linte, Z. Yaniv, Cine cardiac mri slice misalignment correction towards full 3d left ventricle segmentation, in: Medical Imaging 2018: Image-Guided Procedures, Robotic Interventions, and Modeling, vol. 10576, International Society for Optics and Photonics, 2018, p. 1057607.

[9] A.G. Chandler, R.J. Pinder, T. Netsch, J.A. Schnabel, D.J. Hawkes, D.L. Hill, R. Razavi, Correction of misaligned slices in multi-slice cardiovascular magnetic resonance using slice-to-volume registration, J. Cardiovasc. Magn. Reson. 10 (1) (2008) 1–9.
[10] W.P. Segars, G. Sturgeon, S. Mendonca, J. Grimes, B.M. Tsui, 4d xcat phantom for multimodality imaging research, Med. Phys. 37 (9) (2010) 4902–4915.
[11] Philips, IntelliSpace portal 10 (accessed September, 2019). [Online]. Available: https://www.usa.philips.com/healthcare/product, 2018.
[12] S. Amirrajab, et al., A Multipurpose Numerical Late Gadolinium Enhancement Cardiac Mr Image Simulation Tool, ESMRMB, 2020.
[13] F. Guo, P.R. Krahn, T. Escartin, I. Roifman, G. Wright, Cine and late gadolinium enhancement mri registration and automated myocardial infarct heterogeneity quantification, Magn. Reson. Med. 85 (5) (2021) 2842–2855.
[14] A. Fedorov, R. Beichel, J. Kalpathy-Cramer, J. Finet, J.-C. Fillion-Robin, S. Pujol, C. Bauer, D. Jennings, F. Fennessy, M. Sonka, et al., 3d slicer as an image computing platform for the quantitative imaging network, Magn. Reson. Imag. 30 (9) (2012) 1323–1341 (accessed September, 2019). [Online]. Available: https://www.slicer.org/.
[15] K.H. Ten Tusscher, A.V. Panfilov, Alternans and spiral breakup in a human ventricular tissue model, Am. J. Physiol. Heart Circ. Physiol. 291 (3) (2006) H1088–H1100.
[16] J.D. Bayer, R.C. Blake, G. Plank, N.A. Trayanova, A novel rule-based algorithm for assigning myocardial fiber orientation to computational heart models, Ann. Biomed. Eng. 40 (10) (2012) 2243–2254.
[17] C.M. Costa, E. Hoetzl, B.M. Rocha, A.J. Prassl, G. Plank, Automatic parameterization strategy for cardiac electrophysiology simulations, in: In Computing in Cardiology 2013, IEEE, 2013, pp. 373–376.
[18] H. Martinez-Navarro, A. Mincholé, A. Bueno-Orovio, B. Rodriguez, High arrhythmic risk in antero-septal acute myocardial ischemia is explained by increased transmural reentry occurrence, Sci. Rep. 9 (1) (2019) 1–12.